INVESTIGATION ON THE FLOW AND HEAT TRANSFER CHARACTERISTICS OF SUPERCRITICAL CO_2 IN PRINTED CIRCUIT HEAT EXCHANGER WITH ASYMMETRIC AIRFOIL FINS

by

Dan WANG[a], Jiagang LI[a], Kang PAN[a], Luyao WANG[a], and Zunchao LIU[b*]

[a] School of Mechanical and Power Engineering, Zhengzhou University, Zhengzhou, China
[b] School of Aero Engine, Zhengzhou University of Aeronautics, Zhengzhou, China

Original scientific paper
https://doi.org/10.2298/TSCI221224075W

As an essential component of the supercritical CO_2 recompression Brayton cycle, the recuperator has a significant impact on the efficiency and stability of the entire cycle system. The printed circuit heat exchanger is the most suitable heat exchanger for the recuperator in the supercritical CO_2 recompression Brayton cycle. To investigate the effects of the structural parameters of the asymmetric AFF on the thermo-hydraulic performance of the printed circuit heat exchangers, simplified 3-D numerical simulation models for the printed circuit heat exchanger with National Advisory Committee for Aeronautics 85XX series asymmetric AFF were built. An optimization method combining an orthogonal experiment and a quadratic polynomial surrogate model with a multi-objective genetic algorithm was proposed to obtain the optimal structural parameters. The results show that the fin thickness, l_b, has the most significant effect on the comprehensive performance and fluid-flow performance, and the transverse spacing, l_c, has the highest influence on the thermal performance. The optimum structural parameters set are a combination of the transverse spacing of 3.9 mm, the longitudinal spacing of 11.5 mm, and the fin thickness of 0.77mm.

Key words: *supercritical CO_2, printed circuit heat exchanger, asymmetric AFF, thermo-hydraulic performance*

Introduction

The Brayton power cycle using supercritical carbon dioxide (SCO_2) as the working medium has attracted a lot of attention because of its higher energy conversion efficiency than the Rankine cycle [1]. The recompression cycle is the most stable one among the proposed SCO_2 Brayton power cycle layouts [2]. There are two main types of equipment in the recompression cycle, the turbomachines (a main compressor, a re-compressor, and a turbine) and the heat exchangers (a precooler, a low temperature recuperator, a high temperature recuperator, and an intermediate heat exchanger) [3]. As the crucial heat transfer equipment in the SCO_2 recompression Brayton cycle system, the recuperators affect the circulation efficiency and safety of the system substantially and need to operate stably under extreme working conditions [4]. The printed circuit heat exchangers (PCHE) have high resistance to thermal stress and mechanical stress [5] and are considered to be the most suitable heat exchangers for use as recuperators [6, 7] in the SCO_2 recompression Brayton cycle.

* Corresponding author, e-mails: 202022202014027@gs.zzu.edu.cn, zchliu@zzu.edu.cn

Similar to the production of printed circuit boards, these channels in the heat exchanger are made by chemical etching technology, hence the name PCHE is produced [8]. Continuous channels and discontinuous channels are the two main types of channels for PCHE in practical applications. For the research of continuous channels, Ma *et al.* [9] numerically analyzed and compared the performance of the PCHE with zigzag channels, they found that the increased channel inclination angle will lead to increased heat transfer capacity, and the augmentation in heat transfer capacity varies from operating conditions. Saeed and Kim [10] proposed a PCHE with sinusoidal shape flow channels, the results show that the PCHE with sinusoidal shape flow channels can provide 2.5 times improvement in flow performance while maintaining the same amount of heat exchange compared to a PCHE with zigzag flow channels. Aneesh *et al.* [11] conducted a comparison analysis of the thermo-hydraulic performance of the helium gas in straight, triangular, zigzag, and trapezoidal channel PCHE. According to their simulation results, the thermo-hydraulic performance of the four channel structures from high to low is trapezoidal, zigzag, triangular, and straight. Lin *et al.* [12] numerically analyzed the thermal performance and flow characteristics of the PCHE with seven different continuous channels, and the results show that the S-20 channel produces the best thermal performance.

The discontinuous channels are composed of heat transfer plates and the fins on the heat transfer plates. The first type of fin proposed for PCHE is *S*-shape fins, and its advantages of low pressure loss over the zigzag channel PCHE were found by Tsuzuki *et al.* [13]. Then, Kim *et al.* [14] proposed a PCHE using NACA0020 AFF (AFF), and the result show that the NACA0020 AFF can significantly eliminate the pressure drop in the flow channel. To furthermore increase the comprehensive performance of PCHE with AFF, lots of new structures were proposed. Xu *et al.* [15] designed an AFF-based structure named *swordfish fin*. The results show that the swordfish fins can effectively attenuate the impact of the incoming flow on the fin head. A set of AFF with different groove thicknesses is designed by Ma *et al.* [16], the results show that, compared with the NACA0020 AFF, the AFF with a groove thickness of 0.6 mm reduce the pressure drop by up to 15% without affecting the thermal performance of the PCHE. Chu *et al.* [17] tested the performance of the PCHE with the asymmetric NACA8315, NACA8515, and NACA8715 AFF, and the results show that the PCHE with asymmetric AFF has higher heat transfer performance than the PCHE with the symmetric AFF. Wang *et al.* [18] studied the performance of the AFF PCHE with different shapes. The results show that the asymmetric AFF PCHE have better thermo-hydraulic performance than the symmetric AFF PCHE. Besides, the performance of the asymmetric AFF PCHE has been studied for applying in various fields [19-21].

As discussed, the asymmetric AFF PCHE have better thermo-hydraulic performance than the other PCHE. However, the effects of the structural parameters of the asymmetric AFF on the performance of the PCHE are not clear, and the optimal structural parameters of the asymmetric AFF have not been proposed either. Furthermore, the improvement in heat transfer capacity often increases the pressure loss, it is difficult to evaluate the performance of the heat exchanger by a single objective, but the evaluation of the performance of the asymmetric AFF PCHE using the multi-objective optimization method has seldom been conducted in the open literature.

In this paper, the asymmetric AFF PCHE, which have a high potential to be employed as a low temperature recuperator of the SCO_2 recompression Brayton cycle, were numerically studied. The effects of fin thickness and fin arrangement of the NACA85XX series asymmetric AFF on the thermo-hydraulic performance of the PCHE were investigated. An orthogonal experiment with three factors and four levels was designed to obtain the quadratic polynomial surrogate model, which was applied to gain the optimal structural parameters of the asymmetric AFF by combining a multi-objective decision algorithm. The research results provide guidance for the application of PCHE with asymmetric AFF in the SCO_2 recompression Brayton cycle.

Mathematical models

Geometrical model

The main structural parameters of the NACA series AFF are shown in fig. 1(a), where t represents the maximum distance between the chord and the center arc, the value of the relative camber is calculated by dividing t by the chord length l_a and multiplying by 100, the value of the maximum bending position is equal to the distance from the head of the fin to the maximum thickness position of the fin divided by l_a and multiplying by 10, the value of the relative thickness is equal to the maximum thickness l_b divided by the chord length l_a and multiplying by 100.

The front view and 3-D view of the simplified geometric models of the numerical computation are shown in figs. 1(b) and 1(c), respectively. The solid domain includes two parts: the plates and the fins. The plate thickness is 0.68 mm, and the fin thickness is 0.95 mm. To simplify the model, the thickness of the upper and lower plates is half of the thickness of the middle plate, that is, 0.34 mm, and each plate is arranged with 20 fins.

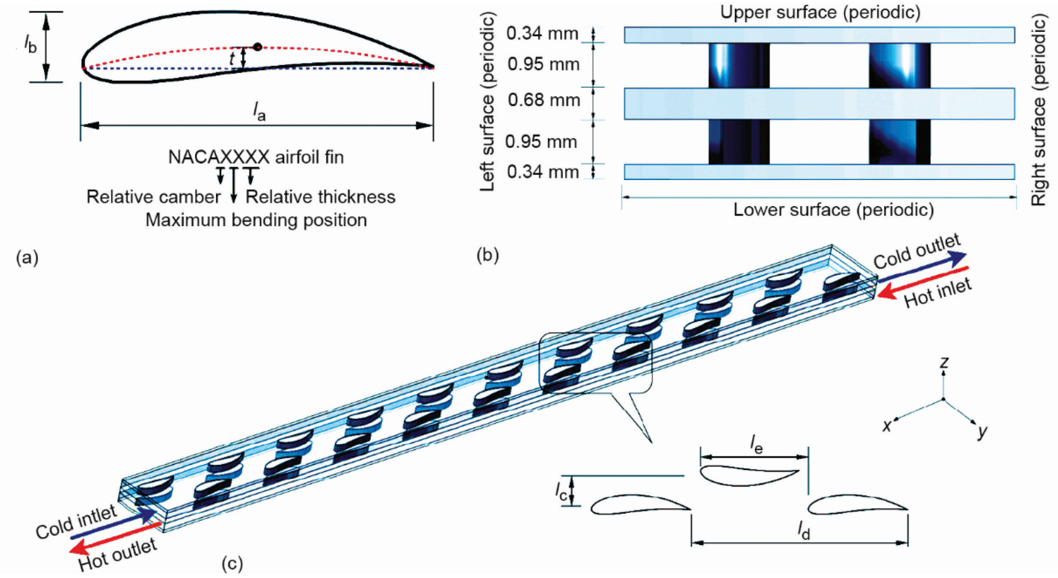

Figure 1. Geometric model; (a) NACA series AFF, (b) front view of computational domain, and (c) 3-D view of computation domains

The flow direction of the hot and cold fluid in the heat exchanger channel is countercurrent, and the orientation of fins in the cold and hot channels is opposite. The fluid domains include one cold fluid and one hot fluid. To provide a uniform velocity and reduce the impact of backflow on calculation accuracy and calculation speed, the inlet and outlet are extended to 12 mm and 18 mm, respectively. The three structural parameters affecting fin arrangement are transverse spacing l_c, longitudinal spacing l_d, and staggered spacing l_e.

Governing equations and parameter definition

The finite volume method is used in this study, and the commercial software ANSYS FLUENT 2021 is employed for the numerical simulations.

Following are the governing equations for fluid.

– Continuity equation:

$$\frac{\partial(\rho u_j)}{\partial x_j} = 0 \tag{1}$$

– Momentum equation:

$$\rho \frac{\partial(u_i u_j)}{\partial x_j} = -\frac{\partial p_i}{\partial xi} + \mu \frac{\partial}{\partial x_j}\left(\frac{\partial u_i}{\partial x_j} + \frac{\partial u_j}{\partial x_i} - \frac{2}{3}\delta_{ij}\frac{\partial u_k}{\partial x_k}\right) \tag{2}$$

– Energy equation:

$$\frac{\partial}{\partial x_j}[u_i(\rho E + p)] = \frac{\partial}{\partial x_i}\left[(k_\mathrm{f} + k_\mathrm{t})\frac{\partial T}{\partial x_i}\right] \tag{3}$$

where k_f is the thermal conductivity of fluid, k_t – the turbulent thermal conductivity, δ_{ij} – the Kronecker delta, and μ – the dynamic viscosity.

The governing equations for solid is:

$$\frac{\partial}{\partial x_j}\left[k_\mathrm{s}\frac{\partial T}{\partial x_j}\right] = 0 \tag{4}$$

where k_s is the thermal conductivity of solid.

Due to the width of the flow channel changes along the flow direction, the following equation is used to calculate the hydraulic diameter:

$$D_\mathrm{h} = \frac{4V_\mathrm{h}}{S} \tag{5}$$

where V_h is the volume of the fluid domain and S – the area of the coupled walls between the fluid and solid.

The Reynold number is:

$$\mathrm{Re} = \frac{mD_\mathrm{h}}{\mu\dfrac{V_\mathrm{h}}{L}} \tag{6}$$

where m is the inlet mass-flow rate of fluid, μ – the dynamic viscosity of the fluid and L – the length of the fluid.

The Nusselt number is:

$$\mathrm{Nu} = \frac{qD_\mathrm{h}}{\lambda(T_\mathrm{w} - T_\mathrm{f})} \tag{7}$$

where T_w is the area-weighted average temperature of the interfaces between the cold fluid domain and the solid domain, T_f – the volume-weighted average temperature of the fluid domain, and q – the heat flux of the coupled walls between the fluid and solid domains.

The friction factor, f, is:

$$f = \frac{\Delta p D_\mathrm{h}}{2\rho u^2 L} = \frac{(p_\mathrm{in} - p_\mathrm{out}) D_\mathrm{h}}{2\rho u^2 L} \tag{8}$$

where p_in and p_out are the pressure of the inlet and outlet, respectively, ρ and u – the density and the velocity of the outlet, respectively.

In this paper, the SST k-ω turbulence model is utilized in the hydrodynamics calculation, the SIMPLE algorithm is selected to couple pressure and velocity, the Least squares cell based method is used to solve variable gradient, and the second order upwind discrete scheme is used to the scattering of the equation. The calculation is considered converged when the residuals of the continuity, momentum, and energy equations are less than 10^{-6}, 10^{-6}, and 10^{-9}, respectively.

Boundary conditions and material properties

The upper and lower surfaces on the z co-ordinate, and the left and right surfaces on the y co-ordinate of the computational model are set as periodic walls. The contact surfaces between fluids and solids are set as coupled walls, and the remaining surfaces are set as adiabatic walls. These types of boundary conditions of walls have been proven to have good efforts when conducting a simulation of the simplified PCHE [4]. The mass-flow inlet and pressure-outlet boundary conditions are used in the inlets and outlets, respectively. The inlet temperature of the cold fluid and hot fluid is 343.15 K and 453.15 K, respectively, and the outlet pressure of the cold fluid and hot fluid is 18 MPa and 8 MPa, respectively. The mass-flow rate of the cold fluid is 0.65 times of that of the hot side. These parameters are selected based on the operating conditions of the low temperature recuperator of the SCO_2 recompression Brayton cycle [22]. The inlet mass-flow rates of the cold fluid are set as 1.9 g/s, 3.8 g/s, 5.7 g/s, 7.6 g/s, 9.5 g/s, and 11.4 g/s, which correspond to the Reynolds numbers of 10000, 20000, 30000, 40000, 50000, and 60000 of the cold fluid of the NACA8510 AFF PCHE when the staggered spacing, longitudinal spacing, and transverse spacing equal to 6 mm, 12 mm, and 4.2 mm, respectively. The Alloy 617 with a density of 8360 kg/m^3, a specific heat capacity of 417 J/kgK, and a thermal conductivity of 21 W/mK is considered as the solid material for PCHE due to its suitability and high endurance at extreme temperature and pressure conditions [23]. Due to the apparent non-linear change of physical property with temperature, the physical data obtained from the NIST (National Institute of Standards and Technology) database are fitted using the ORIGIN software. Finally, the fitted polynomials are imported into the FLUENT software to determine the physical properties of materials. The fitted physical property polynomials and the fitting accuracy R^2 are shown in tab. 1.

As shown in tab. 1, the fitting accuracy R^2 of the fitted polynomials are all close to 1, which means the fitted polynomials have high accuracy and dependability.

Grid generation and verification of grid independence

The multizone method of ANSYS MESHING is used to generate grids, and the grids of the computational domains are shown in fig. 2.

As shown in fig 2, the structured hexahedral grids are generated throughout the computational domains, and the refined grids are generated around the AFF. To test the sensitivity of the calculation results to the grids, the $\Delta p/L$ and q of the NACA8530 AFF PCHE with staggered spacing, longitudinal spacing, and transverse spacing of 6 mm, 12 mm,

Table 1. Fitted physical property polynomials

Scope of application	Physical properties	Polynomials	R^2
p = 8 MPa, 330 K < T < 470 K	Density [kgm^{-3}]	$\rho = 3628.96 - 156.65T + 0.36\times10^{-2}T^2 - 2.75\times10^{-3}T^3$	0.99996
	Specific heat capacity [Jkg^{-1}K^{-1}]	$c_p = 319385.69 - 3027.60T + 10.81T^2 - 1.72\times10^{-2}T^3 + 1.02\times10^{-5}T^4$	0.9957
	Thermal conductivity [Wm^{-1}K^{-1}]	$\lambda = 0.42282 - 2.88\times10^{-3}T + 6.91\times10^{-6}T^2 - 5.38\times10^{-9}T^3$	0.99996
	Kinematic viscosity [m^{2}s^{-1}]	$\nu = 1.18\times10^{-3} - 7.43\times10^{-7}T + 1.82\times10^{-9}T^2 - 1.41\times10^{-12}T^3$	0.99921
p = 18 MPa, 330 K < T < 470 K	Density [kgm^{-3}]	$\rho = 23359 - 156.64T + 0.35757T^2 - 2.75\times10^{-4}T^3$	0.9991
	Specific heat capacity [Jkg^{-1}K^{-1}]	$c_p = -43483.84 - 429.54T - 1.26\,\mathrm{T}^2 + 1.17\times10^{-3}T^3$	0.99786
	Thermal conductivity [Wm^{-1}K^{-1}]	$\lambda = 2.55 - 1.73\times10^{-2}T + 3.99\times10^{-5}T^2 - 3.08\times10^{-8}T^3$	0.99447
	Kinematic viscosity [m^{2}s^{-1}]	$\nu = 2.73\times10^{-3} - 1.92\times10^{-5}T + 4.65\times10^{-8}T^2 - 3.61\times10^{-11}T^3$	0.99935

Figure 2. Grid generation; (a) 3-D view of grids, (b) top view of grids, and (c) front view of grids

and 4.2 mm, respectively, are calculated, and the variations of $\Delta p/L$ and q with the number of grids under a fixed mass-flow rate of the cold fluid of 1.9 g/s are calculated. The rest of the boundary conditions are consistent with those described in chapter *Boundary conditions and material properties*. The results of the grid independence test are shown in tab. 2.

Table 2. Grid independence test

Case	Grid numbers [million]	$\Delta p/L$ [kPam^{-1}]	Deviations [%]	q [kWm^{-2}]	Deviations [%]
1	1.633	2.809	2.646	79.970	3.32
2	3.908	2.704	1.187	80.024	1.01
3	5.221	2.749	0.466	79.942	0.36
4	6.073	2.743	0.224	79.972	0.21
5	6.954	2.736	0	79.943	0

As shown in tab. 2, case 5 is employed as the benchmark. When the number of grids reaches 5.221 million, the deviations of $\Delta p/L$ and q both are less than 1%, so the model with 5.221 million grids is selected for calculation. In addition, the grid size of the heat transfer plate and the two fluids is set as 0.3 mm, and the grid size of the AFF is set as 0.05 mm. 10 rows of the boundary layer grids are built around the AFF, with the first layer being 0.01 mm, and the growth rate being 1.15.

Numerical model validation

Ishizuka *et al.* [24] experimentally tested the fluid-flow and heat transfer performance of the PCHE with zigzag channels using SCO_2 as the working fluid. Based on their experiment, a simplified heat exchanger model consisting of two hot fluids and one cold fluid is established. The experimental PCHE has the following geometrical parameters: hot-side channel pitch equal to 9 mm, bending angle equal to 115°, width of wall equal to 0.6 mm, and diameter equal to 1.9 mm. Cold-side channel pitch equal to 7.24 mm, width of wall equal to 0.7 mm, bending angle equal to 100°, and diameter equal to 1.8 mm. Plate thickness of both cold and hot sides equal to 1.63 mm. The periodic boundary conditions are imposed on the top and bottom walls, and the adiabatic boundary conditions are imposed on the left, right, front, and back walls. The specific values of mass-flow inlet and pressure-outlet boundary conditions are listed in tab. 3, and the comparisons between numerical results and experimental data are shown in tab. 4.

Table 3. Specific values of boundary conditions

$m_{c,\mathrm{in}}$ [gs^{-1}]	$m_{\mathrm{h,in}}$ [gs^{-1}]	$p_{c,\mathrm{out}}$ [MPa]	$p_{\mathrm{h,out}}$ [MPa]	$T_{c,\mathrm{in}}$ [K]	$T_{\mathrm{h,in}}$ [K]
0.3152	0.1445	8.28	2.52	381.05	553.05

Table 4. Comparisons between experimental data and numerical results

	Experimental data	Numerical results	Errors [%]
Δp in cold flow channel [kPa]	73.2	64.4	11.4
Δp in hot flow channel [kPa]	24.1	22.7	6.16
ΔT in cold flow channel [K]	140.3	138.6	1.22
ΔT in hot flow channel [K]	169.6	171.1	0.858

As shown in tab. 4, the maximum error of pressure drop is 11.4% and the maximum error of temperature difference is 1.22%. The errors between the experiment data and numerical results are within the acceptable range, which proves the effectiveness of the calculation method.

Results and discussion

Effects of fin thickness on the thermal and hydraulic performance

In this subsection, the staggered spacing l_e is set as 6 mm, transverse spacing l_c is set as 4.2 mm, and the longitudinal spacing l_d is set as 12 mm, respectively. The variations of the pressure drop per unit length $\Delta p/L$, the heat flux q, and the ratios of q to $\Delta p/L$ of the cold fluid of the PCHE with four different fin thicknesses are shown in fig. 3.

It is worth noting that the fin thicknesses, l_b, of the NACA8510, NACA8520, NACA8530, and NACA8540 AFF are 0.6 mm, 1.2 mm, 1.8 mm, and 2.4 mm, respectively.

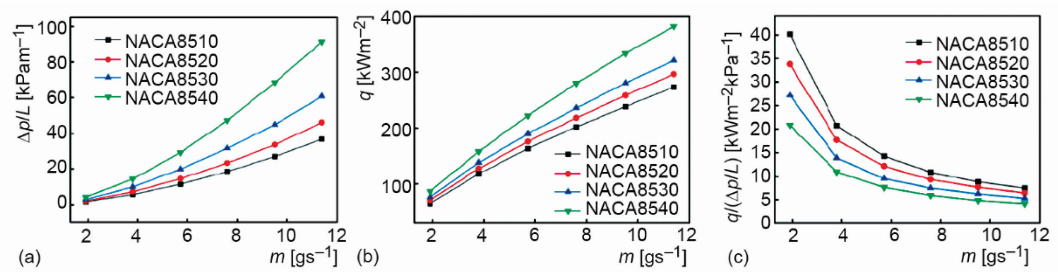

Figure 3. Performance for different fin thicknesses; (a) pressure drop per unit length Δ*p*/*L*, (b) heat flux *q*, and (c) ratios of *q* to Δ*p*/*L*

From fig. 3, it is observed that the increase in fin thickness greatly increases the heat transfer performance of the PCHE but is accompanied by an increase in Δ*p*/*L* and a decrease in the ratios of *q* to Δ*p*/*L*. Tang *et al.* [25] studied the effects of fin thickness on the thermo-hydraulic performance of the PCHE. The results indicate that the increase in fin thickness will enhance the heat transfer performance. However, the mechanism of the effect of fin thickness on the heat transfer performance of the PCHE is still not clear. Therefore, the field synergy principle is introduced to understand the heat transfer improvement mechanism. According to the field synergy principle, the Nusselt number can be written:

$$\mathrm{Nu}_x = \mathrm{Re}_x \,\mathrm{Pr} \int_0^1 (\bar{\mathrm{U}} \nabla \bar{\mathrm{T}})\, \mathrm{d}\bar{\mathrm{y}} \tag{9}$$

$$\bar{\mathrm{U}} \nabla \bar{\mathrm{T}} = \left|\bar{\mathrm{U}}\right| \left|\nabla \bar{\mathrm{T}}\right| \cos \beta \tag{10}$$

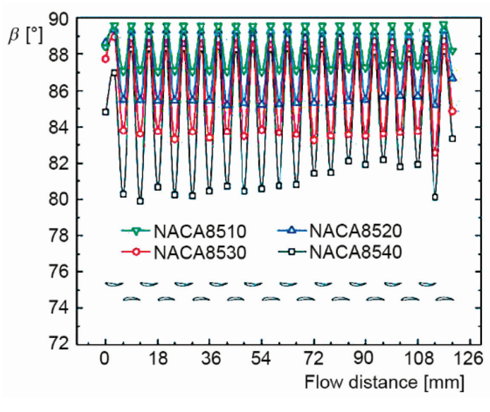

Figure 4. Synergy angle for the PCHE with different fin thickness

where x is the local value, $\bar{\mathrm{U}}$ – the velocity vector, $\nabla \bar{\mathrm{T}}$ – the temperature gradient vector, and β – the synergy angle between the two vectors. The field synergy principle indicates that the smaller the β, the better the heat transfer performance. The 41 isometric cross-sectional planes are created along the flow direction of the cold fluid, and the first cross-sectional plane and the last cross-sectional plane correspond to the head of the first fin and the tail of the last fin, respectively. The synergy angles corresponding to the 41 planes are shown in fig. 4.

As shown in fig. 4, the periodic increase and decrease of the flow cross-sectional area along the flow distance cause the synergy angle vary in a *M-shaped* pattern, where the larger synergy angle corresponds to the middle of the fins and the smaller synergy angle corresponds to the head and tail of the fins. In addition, the NACA8540 AFF correspond to the smallest synergy angle with an average reduction of 1.91%, 3.19%, and 4.28% over the NACA8530, NACA8520, and NACA8510 AFF, respectively. This explains the heat transfer enhancement mechanism of the PCHE with different fin thicknesses.

Effects of fin arrangement on the thermal and hydraulic performance

In this subsection, the effect of fin arrangement on the performance of PCHE is evaluated by comparing the heat flux q and pressure drop per unit length $\Delta p/L$ of the NACA8510 AFF PCHE for longitudinal spacing equal to 12 mm, transverse spacing equal to 4.2 mm and staggered spacing equal to 6 mm. The variations of the values of q and $\Delta p/L$ of the cold fluid for different fin arrangements are shown in figs. 5 and 6, respectively.

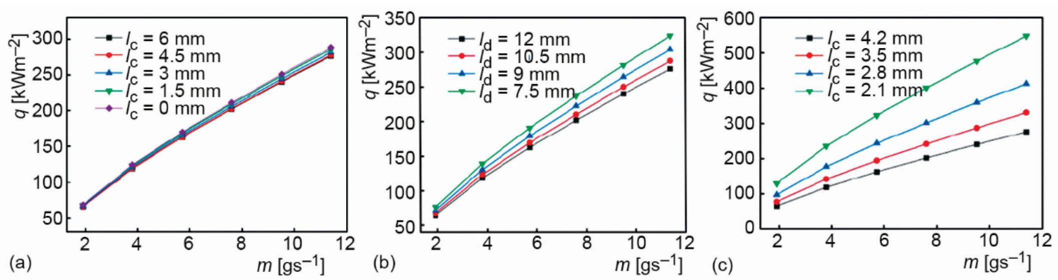

Figure 5. Heat flux q for different fin arrangements; (a) q for different staggered spacing, (b) q for different longitudinal spacing, and (c) q for different transverse spacing

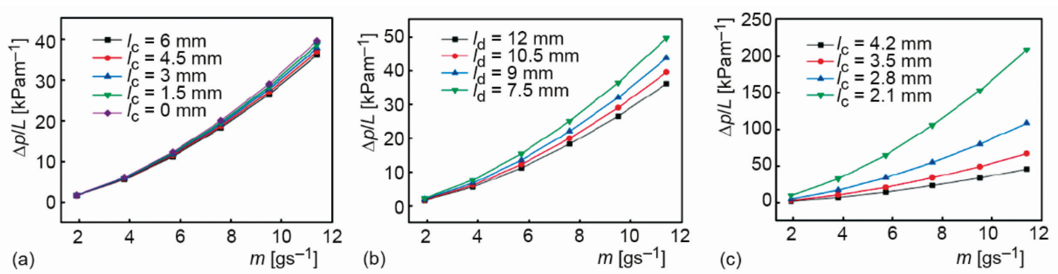

Figure 6. Pressure drops per unit length $\Delta p/L$ for different fin arrangements; (a) $\Delta p/L$ for different staggered spacing, (b) $\Delta p/L$ for different longitudinal spacing, and (c) $\Delta p/L$ for different transverse spacing

As shown in figs. 5 and 6, decreasing the staggered spacing, l_e, longitudinal spacing, l_d, and transverse spacing, l_c, can increase the average values of q by at most 4.5%, 17.3%, and 98.4%, respectively, and can increase the average values of $\Delta p/L$ by at most 9.5%, 37.4%, and 354.4%, respectively. This indicates that the l_c has a greater effect on the fluid-flow and heat transfer performance of the PCHE than the l_e and l_d, the reason for this is the increase in Reynolds number due to the decrease in l_c is the biggest. When the inlet mass-flow rate of cold fluid is 1.9 g/s, the Reynolds numbers of the cold fluid corresponding to the staggered spacing of 0 mm, the longitudinal spacing of 7.5 mm, and the transverse spacing of 2.1 mm are 11425, 15488, and 19611, respectively. As the Reynolds number increases, the inertial forces gradually dominate the fluid-flow and leading to an increase in the Nusselt number and the friction factor. Therefore, for the three spacing affecting the fin arrangement, the reduction of the transverse spacing can increase the heat transfer performance of the PCHE as well as the pressure drop to the greatest extent.

The optimization design of the asymmetric AFF PCHE

The previous study is based on the controlled variable method, and an orthogonal experiment that keeps the inlet mass-flow rate of cold fluid equal to 1.9 g/s is designed to further investigate the effects of asymmetric AFF on the performance of the PCHE. The three factors and four levels of the orthogonal experiment and the experiment results of the orthogonal experiment are shown in tabs. 5 and 6, respectively. Since the staggered spacing, l_e, has a minor effect on the performance of PCHE, the l_e is set as a constant of 4 mm. According to the research by Kim *et al.* [26], the PCHE with longitudinal spacing, l_d, bigger than 12 mm has no enhancement of the heat transfer at the fin, and the pressure drop is large when transverse spacing, l_c, is 2.4 mm. Therefore, the l_d of 7.5 mm, 9 mm, 10.5 mm, and 12 mm are selected, and the l_c of 3 mm, 3.6 mm, 4.2 mm, and 4.8 mm are selected. The fin thicknesses of 0.6 mm, 1.2 mm, 1.8 mm, and 2.4 mm are selected, which is the same as that of the research of Chen *et al.* [27].

Table 5. The factors and the levels

Levels	Factors		
	Transverse spacing [mm]	Longitudinal spacing [mm]	Fin thickness [mm]
1	3	7.5	0.6
2	3.6	9	1.2
3	4.2	10.5	1.8
4	4.8	12	2.4

Table 6. Orthogonal experiment and experiment results

Cases	Transverse spacing [mm]	Longitudinal spacing [mm]	Fin thickness [mm]	Nu	f	Nu/f
1	3	7.5	0.6	91.75	0.0247	3712
2	3	9	1.2	97.06	0.0237	4103
3	3	10.5	1.8	119.8	0.0351	3410
4	3	12	2.4	149.9	0.0551	2721
5	3.6	7.5	1.2	78.93	0.0243	3255
6	3.6	9	0.6	67.49	0.0150	4499
7	3.6	10.5	2.4	117.0	0.0464	2522
8	3.6	12	1.8	91.52	0.0233	3926
9	4.2	7.5	1.8	80.39	0.0315	2554
10	4.2	9	2.4	99.69	0.0449	2221
11	4.2	10.5	0.6	58.82	0.0151	3909
12	4.2	12	1.2	63.27	0.0170	3722
13	4.8	7.5	2.4	90.27	0.0496	1820
14	4.8	9	1.8	63.79	0.0243	2621
15	4.8	10.5	1.2	54.46	0.0169	3211
16	4.8	12	0.6	49.20	0.0126	3890

For the PCHE with identical mass-flow rates, the Nu/*f* can be used to evaluate the comprehensive performance [6, 28]. To intuitively observe the influence of the three factors, the extremum differences and the average values of the Nu, *f*, and Nu/*f* of the cold fluid for the three factors are listed in tab. 7 and fig. 7, respectively. The factor level with the highest average values means the factor level has the highest effect on the corresponding factor, and the extremum difference with the highest value means the corresponding factor has the highest influence on the experiment results.

Table 7. The extremum differences of different factors

Factors	Extremum difference for Nusselt number	Extremum difference for *f*	Extremum difference for Nu/*f*
Transverse spacing	50.21	0.00877	664.96
Longitudinal spacing	6.473	0.00554	729.24
Fin thickness	47.41	0.03210	1681.3

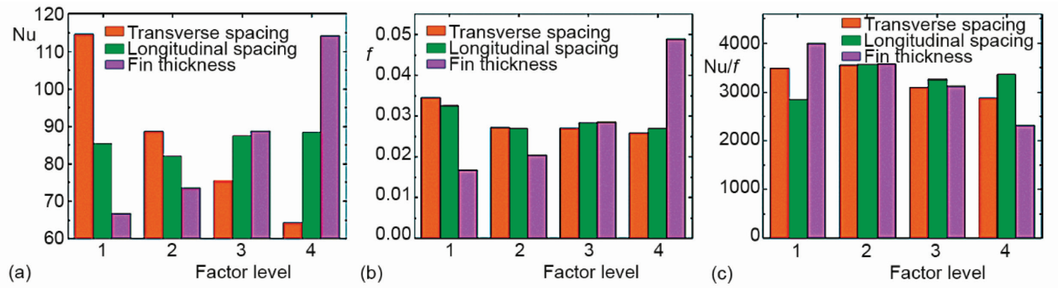

Figure 7. The average values of different factors; (a) average values of Nusselt number, (b) average values of *f*, and (c) average values of Nu/*f*

The results shown in tab. 7 indicate that the transverse spacing has the most significant effect on heat transfer performance, and the fin thickness has the most significant effect on fluid-flow performance and comprehensive performance, respectively. The results shown in fig. 7 demonstrate that, for the Nu/*f*, the optimal factor levels corresponding to the transverse spacing, longitudinal spacing, and fin thickness are 2, 2, and 1, respectively, which indicates that case 6 listed in tab. 6 is the optimal solution of the orthogonal experiment. In order to further describe and predict the relationship between the factors and results, a quadratic polynomial considering the interaction between factors is used as the surrogate model. By fitting the results of the 16 cases obtained from the orthogonal experiment, the highly precise quadratic polynomial model of Nusselt number and *f* are obtained:

$$\mathrm{Nu} = 291.19 - 84.40A - 5.85B + 19.85C - 1.06AB - 8.52AC - 0.082BC + \\ +10.27A^2 + 0.47B^2 + 13.01C^2 (R^2 = 0.996) \tag{11}$$

$$f = 0.12 - 0.02A - 0.01B + 0.0016C - 0.00037AB - 0.004AC - 0.00041BC + \\ +0.0043A^2 + 0.00046B^2 + 0.01168C^2 (R^2 = 0.984) \tag{12}$$

where A, B, and C represent the transverse spacing, longitudinal spacing, and fin thickness, respectively.

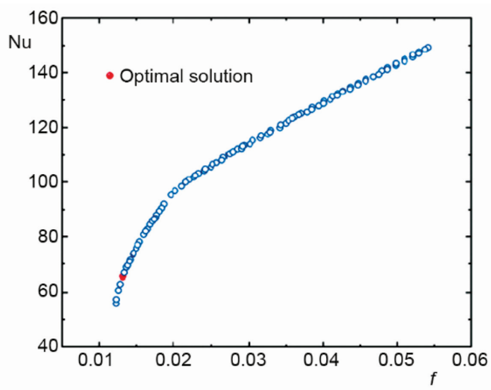

Figure 8. Pareto frontier and optimal solution

Multi-objective genetic algorithms are often used to reconcile each objective function and obtain the Pareto frontier, which includes a set of solutions that make each objective as desirable as possible. In this paper, a fast non-dominated sorting genetic algorithm with an elite retention strategy, the NSGA-II algorithm, is used to optimize Nusselt number and f by combining a quadratic polynomial surrogate model. The program is implemented using the MATLAB software. The parameters of the NSGA-II algorithm are as follows: initial population quantity = 100, maximum number of iterations = 50, crossover probability = 80%, mutation probability = 5%. The values of A range from 3-4.8 mm, the values of B range from 7.5-12 mm, and the values of C range from 0.6-2.4 mm. Then, the optimal solution is selected using the TOPSIS method. The Pareto frontier and the optimal solution are shown in fig. 8.

The optimal combination of structural parameters chosen by TOPSIS is A = 3.9 mm, B = 11.5 mm, and C = 0.77 mm, which reduces Nusselt number by 10.05% and f by 16.41%, and increases Nu/f by 7.61% compared to the optimal solution obtained from the orthogonal experiment. This shows that the improvement of the flow performance of the optimal solution chosen by TOPSIS is greater than the loss of heat transfer performance when compared to the optimal solution obtained from the orthogonal experiment, and the new optimization method is more advantageous than the orthogonal experiment.

In the open literature, several scholars have studied the effects of fin arrangement on the performance of the PCHE and have proposed the optimal fin arrangements [15, 26]. However, their studies considered the fin thickness as a constant, which has a significant influence on the performance of the PCHE [27]. Unlike their studies, this study uses the quadratic polynomial that considers the interaction between the fin thickness and the fin arrangement to obtain the optimal structural parameters. In addition, most of the optimizations performed for the PCHE are single-objective optimizations [18, 21], while the results of this paper show that the newly proposed optimization method can further optimize the performance of the PCHE compared to the optimization considering only a single objective.

Conclusions

The asymmetric AFF PCHE have the potential as a low temperature recuperator of the SCO_2 recompression Brayton cycle. In this paper, a 3-D numerical simulation was conducted to investigate the thermo-hydraulic performance of the PCHE with asymmetric AFF. Using a combination of an orthogonal experiment, a quadratic polynomial surrogate model, and a multi-objective genetic algorithm to obtain the optimal parameters of the asymmetric AFF PCHE. The main conclusions are as follows.

- The increase in fin thickness leads to an increase in the synergy of the velocity vector and temperature gradient, which remarkably enhances the heat transfer performance of the PCHE. Since the decrease in transverse spacing leads to a significant increase in Reynolds number, it has the greatest effect on the heat transfer and fluid-flow performance among the parameters that affect the fin arrangement.

- The heat transfer performance of PCHE is mainly affected by the transverse spacing, followed by the fin thickness, longitudinal spacing has the smallest influence on the heat transfer performance. The fluid-flow performance of PCHE is mainly affected by the fin thickness, followed by the transverse spacing, longitudinal spacing has the smallest influence on the fluid-flow performance.
- The new optimization method proposed in this paper provides a new perspective for the optimization of the PCHE. The optimal solution obtained by the new optimization method is the PCHE with a transverse spacing of 3.9 mm, a longitudinal spacing of 11.5 mm, and a fin thickness of 0.77 mm, whose Nusselt number and f are reduced by 10.05% and 16.41%, respectively, and whose Nusselt number and f is increased by 7.61%, compared with the optimal solution obtained by the orthogonal experiment.

Acknowledgment

The work is supported by the National Natural Science Foundation Program of China (No. 51776190) and the Key Science and Technology Research Projects of Henan Province (No. 212102310577, No. 222102320230).

Nomenclature

c_p – specific heat capacity, [Jkg^{-1}K^{-1}]
D_h – hydraulic diameter, [m]
E – energy, [J]
f – friction factor [= $\Delta p D_\mathrm{h}/2\rho u^2 L$], [–]
k_f – fluid thermal conductivity, [Wm^{-1}K^{-1}]
k_s – solid thermal conductivity, [Wm^{-1}K^{-1}]
k_t – turbulent thermal conductivity
L – length of fluid domain, [m]
l_a – chord length, [mm]
l_b – maximum thickness of fin, [mm]
l_c – transverse spacing, [mm]
l_d – longitudinal spacing, [mm]
l_e – staggered spacing, [mm]
m – mass-flow rate, [gs^{-1}]
Nu – Nusselt number, [= $qD_\mathrm{h}/(T_\mathrm{w} - T_\mathrm{f})\lambda$], [–]
p – pressure, [MPa]
Δp – pressure drop, [Pa]
q – heat flux, [kWm^{-2}]
Re – Reynold number [= $mD_\mathrm{h}/\mu/(V_\mathrm{h}/L)$], [–]
S – area of the interfaces between fluid domain and solid domain, [m^2]
T – temperature, [K]
u – velocity, [ms^{-1}]
V_h – volume of fluid, [m^3]

Greek symbols

ρ – density, [kgm^{-3}]
λ – thermal conductivity, [Wm^{-1}K^{-1}]
ν – kinematic viscosity [m^{2}s^{-1}]
μ – dynamic viscosity [Pa·s]
δ_{ij} – Kronecker delta

Subscripts

c – cold flow channel
f – fluid
h – hot
in – inlet
out – outlet
w – wall

Acronyms

AFF – airfoil fins
NACA – national advisory committee for aeronautics
NIST – national institute of standards and technology
PCHE – printed circuit heat exchanger
TOPSIS – Technique for Order of Preference by Similarity to Ideal Solution

References

[1] Cheng, W. L., *et al.*, Global Parameter Optimization and Criterion Formula of Supercritical Carbon Dioxide Brayton Cycle with Recompression, *Energy Conversion and Management, 150* (2017), Oct., pp. 669-677
[2] Wu, C., *et al.*, Energy, Exergy and Exergoeconomic Analyses of a Combined Supercritical CO_2 Recompression Brayton/Absorption Refrigeration cycle, *Energy Conversion and Management, 148* (2017), Sept., pp. 360-377

[3] Khatoon, S., *et al.*, Modeling and Analysis of Air-Cooled Heat Exchanger Integrated with Supercritical Carbon Dioxide Recompression Brayton Cycle, *Energy Conversion and Management, 232* (2021), 113895
[4] Huang, C. Y., *et al.*, Review on the Characteristics of Flow and Heat Transfer in Printed Circuit Heat Exchangers, *Applied Thermal Engineering*, *153* (2019), May, pp. 190-205
[5] Wang, J., *et al.*, Structural Stress Analysis of Hybrid Heat Exchangers in the S-CO_2 Power Cycle for Marine Waste Heat Recovery, *Thermal Science*, *27* (2022), 1B, pp. 811-823
[6] Li, X. L., *et al.*, A Performance Recovery Coefficient for Thermal-Hydraulic Evaluation of Recuperator in Supercritical Carbon Dioxide Brayton Cycle, *Energy Conversion and Management*, *256* (2022), 115393
[7] Rao, Z. H., *et al.*, Multi-Objective Optimization of Supercritical Carbon Dioxide Recompression Brayton Cycle Considering Printed Circuit Recuperator Design, *Energy Conversion and Management*, *201* (2019), 112094
[8] Fan, Y .L., Luo, L. G., Recent Applications of Advances in Microchannel Heat Exchangers and Multi-Scale Design Optimization, *Heat Transfer Engineering*, *29* (2008), 5, pp. 461-474
[9] Ma, T., *et al.*, Study on Local Thermal-Hydraulic Performance and Optimization of Zigzag-Type Printed Circuit Heat Exchanger at High Temperature, *Energy Conversion and Management*, *104* (2015), Nov., pp. 55-66
[10] Saeed, M., Kim, M. H., Thermal-Hydraulic Analysis of Sinusoidal Fin-Based Printed Circuit Heat Exchangers for Supercritical CO_2 Brayton Cycle, *Energy Conversion and Management*, *193* (2019), Aug., pp. 124-139
[11] Aneesh, A. M., *et al.*, Effects of Wavy Channel Configurations on Thermal-Hydraulic Characteristics of Printed Circuit Heat Exchanger (PCHE), *International Journal of Heat and Mass Transfer*, *118* (2018), Mar., pp. 304-315
[12] Lin, Y. S., *et al.*, Numerical Investigation on Thermal Performance and Flow Characteristics of Z and S Shape Printed Circuit Heat Exchanger Using S-CO_2, *Thermal Science*, *23* (2019), Suppl. 3, pp. S757-S764
[13] Tsuzuki, N., *et al.*, High Performance Printed Circuit Heat Exchanger, *Applied Thermal Engineering*, *27* (2007), 10, pp. 1702-1707
[14] Kim, D. E., *et al.*, Numerical Investigation on Thermal-Hydraulic Performance of New Printed Circuit Heat Exchanger Model, *Nuclear Engineering and Design*, *238* (2008), 12, pp. 3269-3276
[15] Xu, X. Y., *et al.*, Optimization of Fin Arrangement and Channel Configuration in an AFF PCHE for Supercritical CO_2 Cycle, *Applied Thermal Engineering*, *70* (2014), 1, pp. 867-875
[16] Ma, Y., *et al.*, Performance Study on a Printed Circuit Heat Exchanger Composed of Novel AFF for Supercritical CO_2 Cycle Cooling System, *Thermal Science*, *27* (2022), 1B, pp. 891-903
[17] Chu, W. X., *et al.*, Thermo-Hydraulic Performance of Printed Circuit Heat Exchanger with Different Cambered AFF, *Heat Transfer Engineering*, *41* (2019), 8, pp. 708-722
[18] Wang, W., *et al.*, Parametric Study on Thermo-Hydraulic Performance of NACA AFF PCHE Channels, *Energies*, *15* (2022), 14, 5095
[19] Jiang, Q., *et al.*, Adaptive Design Methodology of Segmented Non-Uniform Fin Arrangements for Trans-Critical Natural Gas in the Printed Circuit Heat Exchanger, *Applied Thermal Engineering*, *216* (2022), 119011
[20] Guillen, D. P., *et al.*, Topology Optimization of an AFF Microchannel Heat Exchanger Using Artificial Intelligence, *Nuclear Engineering and Design*, *391* (2022), 111737
[21] Zhu, C. Y., *et al.*, Investigation of the Flow and Heat Transfer Characteristics of Helium Gas in Printed Circuit Heat Exchangers with Asymmetrical AFF, *Applied Thermal Engineering*, *186* (2021), 116478
[22] Ding, M., *et al.*, An Adaptive Flow Path Regenerator Used in Supercritical Carbon Dioxide Brayton Cycle, *Applied Thermal Engineering*, *138* (2018), June, pp. 513-522
[23] Meshram, A., *et al.*, Modeling and Analysis of a Printed Circuit Heat Exchanger for Supercritical CO_2 Power Cycle Applications, *Applied Thermal Engineering*, *109* (2016), Oct., pp. 861-870
[24] Ishizuka, T., *et al.*, Thermal-Hydraulic Characteristics of a Printed Circuit Heat Exchanger in a supErcritical CO_2 Loop, (ed. Herve Lemonnier), *Proceedings,* The 11th International Topical Meeting on Nuclear Reactor Thermal-Hydraulics (NURETH-11), Avignon, France, 2005, pp. 218-232
[25] Tang, L., *et al.*, Optimization of Fin Configurations and Layouts in a Printed Circuit Heat Exchanger for Supercritical Liquefied Natural Gas Near the Pseudo-Critical Temperature, *Applied Thermal Engineering*, *172* (2020), 115131

[26] Kim, T. H., *et al.*, Numerical Analysis of Air-Foil Shaped Fin Performance in Printed Circuit Heat Exchanger in a Supercritical Carbon Dioxide Power Cycle, *Nuclear Engineering and Design*, *288* (2015), July, pp. 110-118
[27] Chen, F., *et al.*, Comprehensive Performance Comparison of AFF PCHE with NACA 00XX Series Airfoil, *Nuclear Engineering and Design*, *315* (2017), Apr., pp. 42-50
[28] Fan, J. F., *et al.*, A Performance Evaluation Plot of Enhanced Heat Transfer Techniques Oriented for Energy-Saving, *International Journal of Heat and Mass Transfer*, *52* (2009), 1-2, pp. 33-34

Paper submitted: December 24, 2022
Paper revised: February 9, 2023
Paper accepted: February 13, 2023